Journal of Solid State Chemistry 182 (2009) 2791–2795

Contents lists available at ScienceDirect

Journal of Solid State Chemistry

journal homepage: www.elsevier.com/locate/jssc

Rational synthetic strategy: From ZnO nanorods to ZnS nanotubes

Ran Yi [a], Guanzhou Qiu [a], Xiaohe Liu [a,b,*]

[a] Department of Inorganic Materials, Central South University, Changsha, Hunan 410083, People's Republic of China
[b] State Key Laboratory of Powder Metallurgy, Central South University, Changsha, Hunan 410083, People's Republic of China

ARTICLE INFO

Article history:
Received 13 June 2009
Received in revised form
20 July 2009
Accepted 22 July 2009
Available online 30 July 2009

Keywords:
ZnO
ZnS
Core/shell structures
Nanotubes
Optical properties

ABSTRACT

We demonstrate here that ZnS nanotubes can be successfully synthesized via a facile conversion process from ZnO nanorods precursors. During the conversion process, ZnO nanorods are first prepared as sacrificial templates and then converted into tubular ZnO/ZnS core/shell naonocomposites through a hydrothermal sulfidation treatment by using thioacetamide (TAA) as sulfur source. ZnS nanotubes are finally obtained through the removal of ZnO cores of tubular ZnO/ZnS core/shell naonocomposites by KOH treatment. The photoluminescence (PL) characterization of the as-prepared products shows much enhanced PL emission of tubular ZnO/ZnS core/shell nanocomposites compared with their component counterparts. The probable mechanism of conversion process is also proposed based on the experimental results.

1. Introduction

During the past decades, wide band gap semiconductor materials have attracted considerable attention due to their size-dependent properties and important technological applications. In particular, ZnS is one of the important semiconductor materials with a wide band gap of 3.7 eV and received a wide range of research interest because of its potential applications in various fields such as nonlinear optical devices, displays, sensors, infrared windows, and lasers [1–3]. Various synthetic routes, for example, solvothermal procedure, hydrothermal method, solid–vapor deposition technique, pulsed laser vaporization [4–6], have been employed to prepare ZnS with different morphologies like nanobelts, nanorods, nanowires, nanoribbons, hollow nanospheres, and other hierarchical nanostructures [7–12]. Recently, a new approach to the preparation of ZnS and ZnS nanocomposites with various morphologies based on corresponding ZnO precursors has been a focus of materials research. Hexagonal ZnS nanotubes have been obtained via a conversion and etching process of ZnO nanocolumns [13]. ZnO/ZnS nanocable and ZnS nanotube arrays have been successfully synthesized by a thioglycolic acid-assisted solution route with removal of ZnO cores [14] and by the conversion from ZnO nanorods due to the Kirkendall effect under simple ultrasonic irradiation [15], respectively. ZnO/ZnS core/shell microspheres have been prepared with ZnO microspheres as reactive templates and they exhibit a distinct enhancement of photoluminescence compared with the uncoated ZnO microspheres [16]. ZnS hollow nanospheres with nanoporous shell were successfully synthesized through the evolvement of ZnO nanospheres [12]. Heterostructured ZnO/ZnS core/shell nanotube arrays were synthesized by a conversion process from ZnO nanorod arrays grown by atomic-layer deposition [17]. The examples above are generally two-step routes while there are still other reports on one-pot process in which ZnO precursors were not point out by the authors but the conversion from ZnO to ZnS was most likely one of the growth mechanisms. For example, hollow ZnS microspheres [18], bifunctional ZnO/ZnS nanoribbons decorated by γ-Fe_2O_3 clusters [19], and flowerlike ZnS–ZnO heterogeneous microstructures built up by ZnS-particle-strewn ZnO microrods [20]. However, there are few reports of tubular ZnO/ZnS core/shell nanocomposites and ZnS nanotubes using ZnO nanorods precursors via a hydrothermal route.

In this paper, tubular ZnO/ZnS core/shell nanocomposites could be successfully obtained via a sulfidation conversion by using ZnO nanorods as sacrificial templates in which thioacetamide (TAA) was used as sulfur source. ZnS nanotubes could also be successfully obtained via an alkali treatment process of tubular ZnO/ZnS core/shell nanocomposites. Compared with ZnO nanorods, as-prepared ZnO/ZnS core/shell nanocomposites and ZnS nanotubes exhibit much different room-temperature photoluminescence (PL) properties. The possible formation mechanism of tubular ZnO/ZnS core/shell nanocomposites was also proposed. This strategy may provide more opportunities for the preparation of core/shell structured and hollow metal chalcogenides.

* Corresponding author at: Department of Inorganic Materials, Central South University, Changsha, Hunan 410083, People's Republic of China.
Fax: +86 7318879815.
E-mail address: liuxh@mail.csu.edu.cn (X. Liu).

0022-4596/$ - see front matter © 2009 Elsevier Inc. All rights reserved.
doi:10.1016/j.jssc.2009.07.038

2. Experimental section

All chemicals were of analytical grade from Shanghai Chemical Reagents Co., and used as starting materials without further purification.

2.1. Preparation of ZnO nanorods

In a typical procedure, 0.297 g of $Zn(NO_3)_2 \cdot 6H_2O$ and 0.142 g of Na_2SO_4 were loaded into a Teflon-lined stainless steel autoclave of 50 ml capacity and dissolved in 30 ml deionized water. Then 5.0 ml of hydrazine monohydrate (80% v/v) solution was added dropwise during vigorous stirring. Next, the autoclave was filled with deionized water up to 80% of the total volume, after 10 min stirring, sealed and maintained at 180 °C for 24 h. Subsequently, the system was allowed to cool to room temperature naturally. The resulting precipitate was collected by filtration and washed with absolute ethanol and distilled water in sequence for several times. The final product was dried in a vacuum box at 50 °C for 4 h.

2.2. Preparation of tubular ZnO/ZnS core/shell nanocomposites

ZnO nanorods (0.081 g) and thioacetamide (TAA, 0.075 and 0.75 g, respectively) were put into a Teflon-lined stainless steel autoclave of 50 ml capacity and dissolved in 30 ml deionized water. The solution was stirred vigorously for 10 min and sealed and maintained at 100 °C for 6 h, and then cooled down to room temperature. The resulting precipitate was collected by filtration and washed with absolute ethanol and distilled water in sequence for several times. The final product was dried in a vacuum box at 50 °C for 4 h.

2.3. Preparation of ZnS nanotubes

Tubular ZnO/ZnS core/shell nanocomposites (0.01 g) were soaked in KOH solution (4 mol/l) under constant stirring for 1 h at room temperature. Finally, the obtained products were collected by centrifugation and washed with distilled water repeatedly and then dried in vacuum box at 50 °C for 4 h.

2.4. Characterization

The obtained products were characterized on a D/max2550 VB+X-ray powder diffractometer (XRD) with Cu$K\alpha$ radiation ($\lambda = 1.54178$ Å). The operation voltage and current were kept at 40 kV and 40 mA, respectively. The size and morphology of the as-synthesized products were determined at 20 kV by a XL30 S-FEG scanning electron microscope (SEM) and at 160 kV by a JEM-200CX transmission electron microscope (TEM) and a JEOL JEM-2010F high-resolution transmission electron microscope (HRTEM). Energy-dispersive X-ray spectroscopy (EDS) was taken on the SEM. The room-temperature photoluminescence (PL) measurement was carried out on an F-2500 spectrophotometer using the 325 nm excitation line of Xe light. ZnO nanorods, ZnO/ZnS core/shell nanocomposites and ZnS nanotubes powder were used as the standards. UV–Vis absorption spectra (UV–Vis) were performed on a Perkin-Elmer Lambda-20 spectrometer at room temperature. For UV spectroscopic analysis samples were dispersed thoroughly in distilled water.

3. Results and discussion

The crystal structure and crystallinity of the as-prepared products were investigated by XRD. Fig. 1(a) shows a typical XRD pattern of ZnO precursors, in which all the diffraction peaks can be well indexed to hexagonal ZnO with lattice constants $a = 3.249$ Å and $c = 5.208$ Å, in good agreement with the standard PDF data (JCPDS file 36–1451). The XRD patterns of tubular ZnO/ZnS core/shell nanocomposites prepared with different molar ratios of ZnO to TAA were shown in Fig. 1(b) and (c), respectively. Besides those of ZnO, characteristic diffraction peaks corresponding to face-centered cubic ZnS can be observed after the sulfidation treatment of ZnO precursors, indicating the formation of ZnO/ZnS nanocomposites. The intensity of main diffraction peaks of ZnS in Fig. 1(c) is much stronger than that in Fig. 1(b), showing more ZnS was formed after sulfidation treatment due to the larger molar ratio of ZnO to TAA. Fig. 1(d) shows the XRD patterns of ZnS nanotubes obtained via an alkali treatment process of tubular ZnO/ZnS core/shell nanocomposites (Fig. 1(c)). The main diffraction peaks in the pattern can be indexed as the face-centered cubic ZnS with lattice constants $a = 5.406$ Å (space group: $F\bar{4}3m(216)$), which are consistent with the values in the literature (JCPDS file 05-0566). The average nanocrystallite size of ZnS products is estimated to be about 2.8 nm by employing the well-known Debye–Scherrer formula, close to exciton Bohr radius of ZnS (about 2.5 nm) [21].

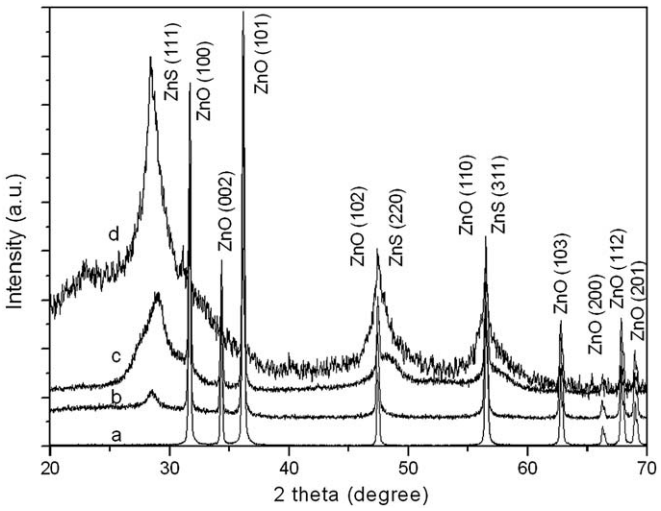

Fig. 1. XRD patterns of the as-prepared ZnO nanorods (a), tubular ZnO/ZnS core/shell nanocomposites obtained with different molar ratios of ZnO to TAA: (b) 1:1, (c) 1:10, and ZnS nanotubes (d).

The morphology, structure, and size of ZnO nanorods were characterized with SEM, TEM and HRTEM. Fig. 2(a) and (b) shows typical low and high magnification SEM images of ZnO precursors, respectively, in which large quantities of ZnO nanorods with diameter in the range of 100–800 nm and length up to 10 μm can be clearly observed. EDS analysis (Fig. S1 of supporting materials) exhibits the products only consist of Zn and O in addition to C which is caused by the C substrate, consistent with XRD characterization. Fig. 2(c) is a representative TEM image of ZnO nanorods, which shows the morphology of several nanorods is relatively straight. Detailed information regarding to the crystal structure of final products has been investigated by HRTEM. Fig. 2(d) shows a typical HRTEM image of an individual ZnO nanorod. The lattice spacing was calculated to be 0.52 nm, corresponding to the *d*-spacing of (0001) crystal plane of the wurtzite ZnO, which suggests that those nanorods are single crystalline and grow along the [0001] direction. The inset of Fig. 2(d) is the corresponding fast Fourier transform (FFT) image of HRTEM result, showing that the nanorod is of single-crystalline structure with preferential [0001] growth direction.

The conversion from ZnO to ZnO/ZnS core/shell nanocomposites can be realized due to the much different solubility between them (solubility product constant K_{sp}: 6.8×10^{-17} for ZnO and 1.2×10^{-24} for ZnS) at the same temperature [18]. Fig. 3(a) depicts a typical low magnification SEM image of ZnO/ZnS core/shell nanocomposites prepared with molar ratio of ZnO to TAA as 1:10, in which many tube-like products with average length about 5 μm can be found. Compared with ZnO nanorod precursors, those products are shorter in length while the diameter is nearly same, indicating ZnO nanorods have broken into smaller sections during the conversion process. Fig. 3(b) is a high magnification SEM image selected from Fig. 3(a). A tube-like product with irregular open tip can be clearly observed. Fig. S1 (refer to supporting materials) shows the result of EDS analysis in which S was found besides Zn and O, agreeing with the XRD pattern. The as-prepared products have also been investigated by TEM and the result is shown in Fig. 3(c). The distinct hollow interior spaces reveal the core/shell structured nature of as-prepared products. In contrast to the smooth inner surface, the outer surface of ZnS shell is relatively rough. Parts of ZnO cores connected with shells can be found with careful observation, as marked by a white rectangle. Two kinds of electron diffraction patterns can be clearly observed (Fig. 3(d)), of which one is indexed to single-crystalline ZnO core and the other refers to ZnS shell with polycrystalline structure, further confirming the core/shell structure of products. A comparative experiment has been carried out to study the influence of the amount of TAA on the morphology of final products and it is found that less TAA leads to the blurred boundaries between cores and shells which are difficult to distinguish (see supporting materials for details).

Since ZnO has an amphoteric character and ZnS exhibits a good resistivity to alkaline solution [18], strong base such as KOH can be employed to remove the ZnO cores while leave the ZnS shells intact. Fig. 4(a) is a typical SEM image of ZnS product obtained with the removal of ZnO cores by KOH treatment. Herein, ZnS nanotubes with open tips can be clearly observed. In addition, the walls of some nanotubes are so thin that they look almost transparent, further confirming the hollow nature of products. There also exist some fragments, which can be attributed to the inevitable collapse of ZnS nanotubes during the removal process due to their relatively thin walls, similar to the collapse of final products in other chemical conversion process such as galvanic replacement in our previous study [22]. Fig. 4(b) shows a higher magnification SEM image exhibiting clearly the open tips of nanotubes. The rough outer surface of nanotubes can also be observed, suggesting the morphology has been well inherited from the shells of ZnO/ZnS core/shell nanocomposites. EDS spectrum of ZnS nanotubes presents prominent Zn and S peaks

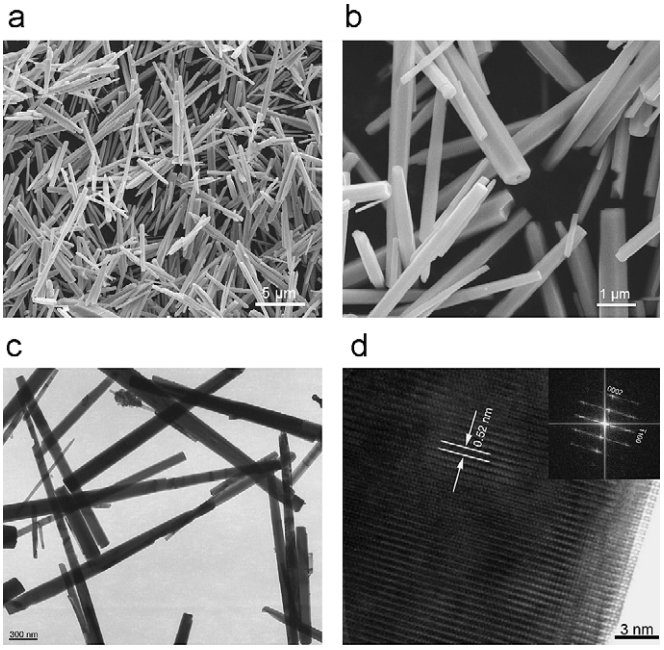

Fig. 2. (a) Low- and (b) high-magnification SEM images, (c) TEM images, and (d) HRTEM image of the as-prepared ZnO nanorods. Inset of (d) fast Fourier transform (FFT) image of the HRTEM result.

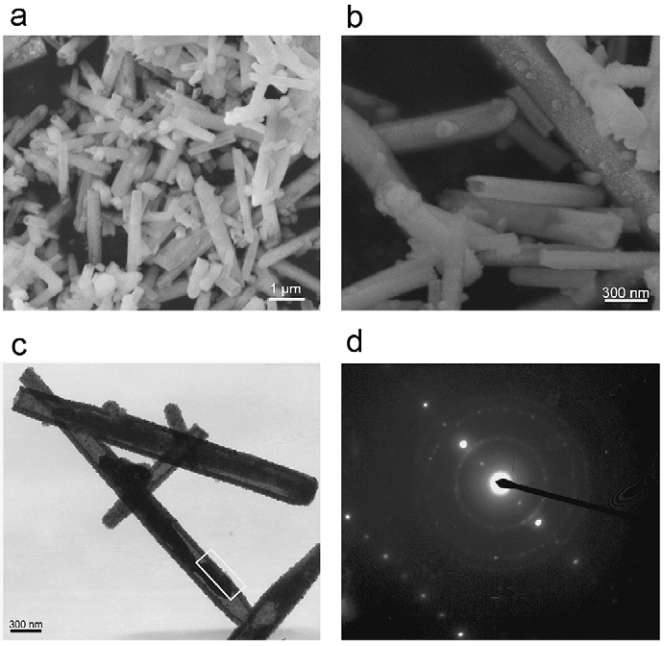

Fig. 3. (a) Low- and (b) high-magnification SEM images, (c) TEM images, and (d) SAED patterns of the as-prepared ZnO/ZnS core/shell nanocomposites obtained with molar ratio of ZnO to TAA as 1:10.

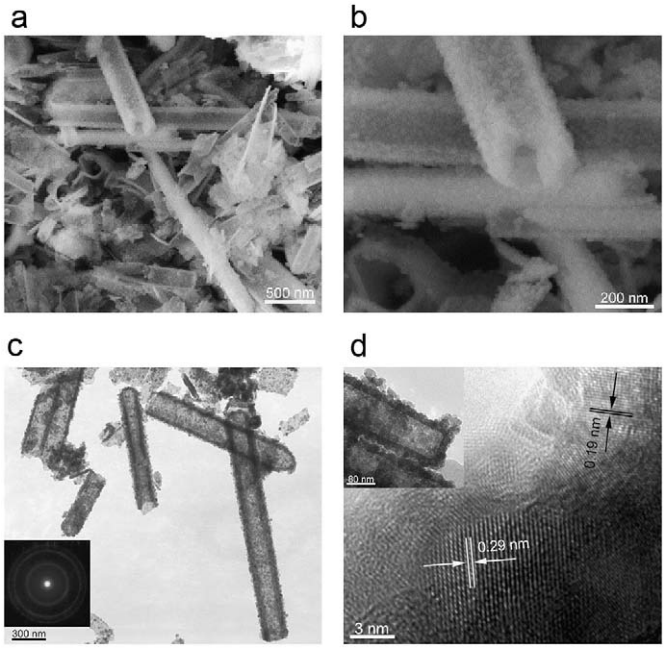

Fig. 4. (a) Low- and (b) high-magnification SEM images, (c) TEM image, and (d) SAED pattern of as-prepared ZnS nanotubes. Inset of (c) SAED pattern and inset of (d) high magnification TEM image of the corresponding product.

(see supporting materials; C and Cu peaks are derived from substrates and weak O peaks may be ascribed to oxygen adsorption). Fig. 4(c) is a representative TEM image of the as-prepared product, in which ZnS nanotubes with lengths ranging from 500 nm to 2 μm and average diameter of 300 nm can be found. The average thickness of the wall of those nanotubes is estimated to be approximately 50 nm. Moreover, the surface of those nanotubes is rough and some fragments exist, consistent well with the SEM observation. The inset of Fig. 4(c) is the corresponding SAED pattern taken on a single nanotube, revealing the polycrystalline nature of the product. The diffraction rings can be outwards indexed to (111), (220), and (311) crystal planes of cubic ZnS, respectively. The inset of Fig. 4(d) is a high magnification TEM image which exhibits that a single ZnS nanotube with a closed tip is built up of numerous nanoparticles and some particles are loosely stacked on the wall of the tube. HRTEM analysis provides further insight into the structures of those nanoparticles. Fig. 4(d) shows a HRTEM image taken on the edge of an individual ZnS nanotube, in which many tiny nanocrystallites can be observed and lattice spacings corresponding to (101) and (110) crystal planes of cubic ZnS are distinguished, providing further evidence for the polycrystalline nature of ZnS nanotubes, agreeing well with the SAED patterns. The nanocrystallite size of ZnS is clearly shown in another HRTEM image and it comes out to be 3 nm (see supporting materials for details), consistent with the estimation from the Debye–Scherrer formula.

The conversion process from ZnO nanorods to ZnS nanotubes which involves sulfidation and etching steps is shown in Fig. 5(a). The conversion from solid templates to core/shell or hollow nanostructures is interesting and several formation mechanisms have been proposed to elucidate the process, including the well-known Ostwald ripening [23], classic and newly prevalent Kirkendall effect [24], and inequivalent exchange of metallic atoms regarding the galvanic replacements reaction, and so on [25]. We believe that a diffusion and consumption process could explain well the formation of ZnO/ZnS core/shell nanocomposites in our case. Fig. 5(b) is the schematic illustration of formation mechanism of ZnO/ZnS core/shell nanocomposites, which presents more details. In the initial stage, TAA reacts with water when it is introduced at certain temperature to produce H_2S, and thus ions exchange happens as S^{2-} react with Zn^{2+} slowly dissolved from the surface of ZnO nanorods to form initial ZnS shells under the driving force caused by the fact that ZnS is more thermodynamically stable due to its lower solubility [16]. Small gaps will form between the ZnO cores and initial ZnS shells as ZnO on the surface is gradually converted into ZnS. Meanwhile, part of ZnO in contact with ZnS shells stochastically remains (Fig. 3(c)) and serves as convenient transportation channels, similar to bridges, for Zn ions to reach the reaction interface via surface and bulk diffusion process. Then zinc ions continuously diffuse from inside of ZnO cores to the outer surface of the ZnS shells along certain ZnO bridges—it is more easy for Zn^{2+} to penetrate through the ZnS shells than S^{2-} does due to the smaller size of Zn^{2+} to react with S^{2-} in solution and thus ZnS shells become thicker as more and more ZnS nanoparticles pile up on the initial ZnS shells. Note some ZnS nanoparticles which do not act as building units of ZnS shells but exist separately in the solution (Fig. 4(d)). With the proceeding of the conversion reaction, the intermediate gap is enlarged due to the continuous consumption of ZnO cores and ZnO/ZnS core/shell nanocomposites are obtained correspondingly. When the core/shell nanocomposites are etched by KOH, the cores are removed and ZnS nanotubes finally form.

Fig. 6 presents the UV–Vis absorption spectra of tubular ZnO/ZnS core/shell nanocomposites prepared with different molar ratios of ZnO to TAA and ZnS nanotubes. The peak at 317 nm can be indexed to ZnS absorption peak, showing an obvious blue shift from 345 nm for bulk ZnS, which is due to the quantum size effects. The peak attributed to ZnO at 378 nm can be found in Fig. 6(a) and (b) which corresponds to ZnO cores in core/shell nanocomposites, and no such a peak but the peak at 378 nm is observed in Fig. 6(c), suggesting the removal of ZnO cores and the existence of ZnS shells.

The room-temperature photoluminescence (PL) under the excitation wavelength of 325 nm has been performed to investigate the optical properties of the as-prepared products. Fig. 7(a) presents the PL spectrum of ZnO nanorods, in which a broad ultraviolet emission with peak at 387 nm, a weak blue band, and a negligible green band can be observed. The ultraviolet emission originates from the excitonic recombination corresponding to the near-band edge emission of ZnO and the green luminescence can be attributed to the recombination of an electron and a photogenerated hole caused by surface defects and oxygen vacancies [26,27] while the exact mechanism in regard to blue emission is not yet clear [28]. Compared with ZnO nanorods, both of ZnO/ZnS core/shell nanocomposites prepared with different molar ratios of ZnO to TAA exhibit much enhanced ultraviolet and visible emissions, similar to the previous report [29]. In addition,

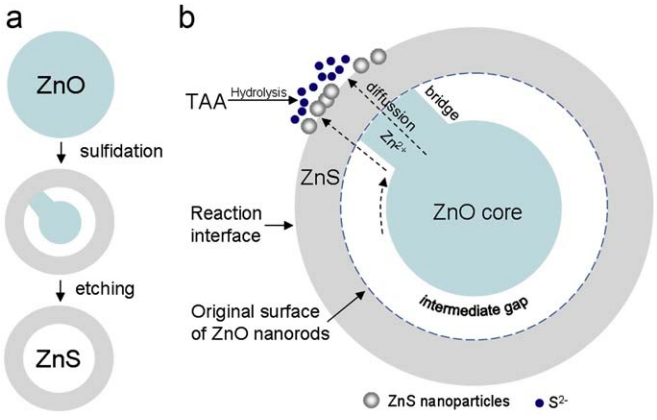

Fig. 5. Schematic illustration of (a) the conversion process from ZnO nanorods to ZnS nanotubes and (b) formation mechanism of ZnO/ZnS core/shell nanocomposites.

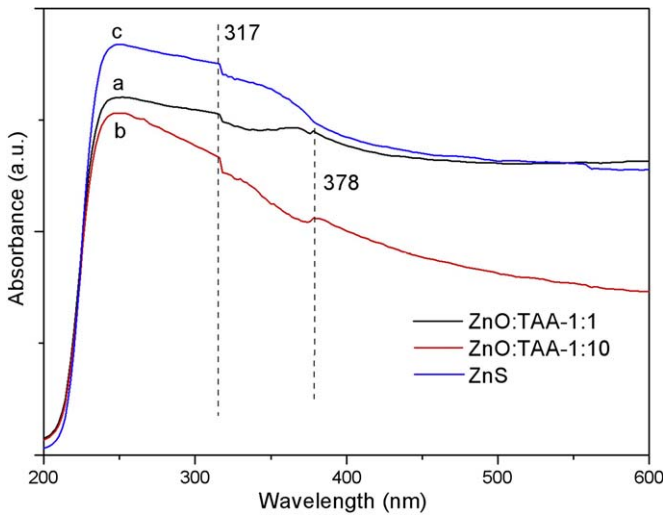

Fig. 6. UV–Vis absorption spectra of ZnO/ZnS core/shell nanocomposites prepared with different molar ratios of ZnO to TAA: (a) 1:1, (b) 1:10, and ZnS nanotubes (c).

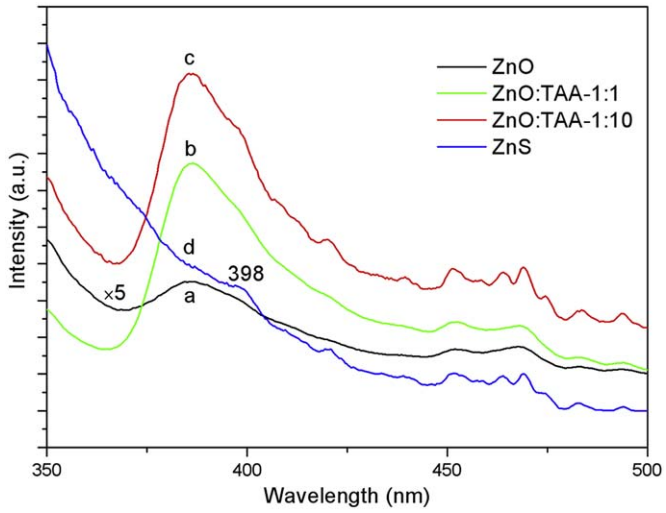

Fig. 7. Photoluminescence spectra of ZnO nanorods (a), ZnO/ZnS core/shell nanocomposites prepared with different molar ratios of ZnO to TAA: (b) 1:1, (c) 1:10, and ZnS nanotubes (d) under the photon excitation of 325 nm at room temperature.

no obvious red- or blue-shift is observed (ultraviolet emission peaks at 386 and 385 for Fig. 7(b) and (c), correspondingly) compared with Fig. 7(a). It is also found that all of the emission peaks in Fig. 7(c) are stronger than those in Fig. 7(b). The portion of ZnS shells with a wider band gap closely coated on ZnO cores provides an efficient passivation of the surface trap states, giving rise to a strongly enhanced fluorescence quantum yield and thus resulting in the obvious enhancement in the ultraviolet emission of core/shell ZnO/ZnS nanocomposites [16,30,31]. The improved PL emission has also been reported in the study of CdS/ZnS wires and CdSe/CdS/ZnCdS/ZnS nanostructures [32,33]. Moreover, the PL properties of ZnS nanotubes have been investigated and the result is shown in Fig. 7(d). Several blue emission bands similar to those in Fig. 7(c) can be seen, except for the weaker intensity. Moreover, a broad emission peak centered at 398 nm was observed in PL spectrum of ZnS nanotubes, showing a remarkable blue shift compared with emission position of bulk ZnS (440–500 nm) [34], which could be attributed to the quantum size effects of ZnS nanocrystallines. The comparison among those spectra suggests that the PL properties of ZnO/ZnS core/shell nanocomposites are superior to their component counterparts.

4. Conclusion

In summary, ZnS nanotubes could be successfully prepared through a facile conversion strategy. ZnO/ZnS core/shell nanocomposites were obtained via a sulfidation process by using ZnO nanorods as sacrificial templates. A subsequent removal process of ZnO cores with KOH treatment finally converts ZnO/ZnS core/shell nanocomposites to ZnS nanotubes. PL study reveals that ZnO/ZnS core/shell nanocomposites exhibit enhanced UV and visible emissions compared with ZnO nanorods and ZnS nanotubes, showing their unique and superior optical properties. A diffusion and consumption mechanism has been proposed for the formation of ZnO/ZnS core/shell nanocomposites. This strategy may be extended to prepare other hollow and core/shell structured metal chalcogenides by using corresponding metal oxides with specific morphologies as precursors.

Supporting information available

SEM images, TEM images, and EDS spectrum of the as-prepared ZnO and ZnO/ZnS core/shell nanocomposites obtained with molar ratio of ZnO to TAA as 1:10 and 1:1, and EDS spectrum of the as-prepared ZnS nanotubes are shown in supporting information.

Acknowledgments

Financial support of this work by National Natural Science Foundation of China (no. 50504017) and Hunan Provincial Key Science and Technology Project of China (no. 2007FJ3008) is gratefully acknowledged.

Appendix A. Supplementary material

Supplementary data associated with this article can be found in the online version at doi:10.1016/j.jssc.2009.07.038.

References

[1] D. Moore, Z.L. Wang, J. Mater. Chem. 16 (2006) 3898.
[2] P. Hu, Y. Liu, L. Fu, L. Cao, D. Zhu, J. Phys. Chem. B 108 (2004) 936.
[3] G.Z. Shen, Y. Bando, D. Golberg, J. Phys. Chem. B 110 (2006) 20777.
[4] S. Yu, M. Yoshimura, Adv. Mater. 14 (2002) 296.
[5] Y. Zhang, Q. Peng, X. Wang, Y.D. Li, Chem. Lett. 33 (2004) 1320.
[6] Q.H. Xiong, G. Chen, J.D. Acord, X. Liu, J.J. Zengel, H.R. Gutierrez, J.M. Redwing, L.C. Lew Yan Voon, B. Lassen, P.C. Eklund, Nano Lett. 4 (2004) 1663.
[7] M.V. Limaye, S. Gokhale, S.A. Acharya, S.K. Kulkarni, Nanotechnology 19 (2008) 415602.
[8] C. Ma, M. Moore, J. Li, Z.L. Wang, Adv. Mater. 15 (2003) 228.
[9] X.S. Fang, L.D. Zhang, J. Mater. Sci. Technol. 22 (2006) 721.
[10] S. Kar, S. Chaudhuri, J. Phys. Chem. B 109 (2005) 3298.
[11] C.H. Liang, Y. Shimizu, T. Sasaki, H. Umehara, N. Koshizaki, J. Phys. Chem. B 108 (2004) 9728.
[12] H.F. Shao, X.F. Qian, Z.K. Zhu, J. Solid State Chem. 178 (2005) 3522.
[13] L. Dloczik, R. Engelhardt, K. Ernst, S. Fiechter, I. Sieber, R. Könenkamp, Appl. Phys. Lett. 78 (2001) 3687.
[14] C.L. Yan, D.F. Xue, J. Phys. Chem. B 110 (2006) 25850.
[15] H.F. Shao, X.F. Qian, B.C. Huang, Mater. Lett. 61 (2007) 3639.
[16] Y.F. Zhu, D.H. Fan, W.Z. Shen, J. Phys. Chem. C 112 (2008) 10402.
[17] H.C. Liao, P.C. Kuo, C.C. Lin, S.Y. Chen, J. Vac. Sci. Technol. B 24 (2006) 2198.
[18] C.L. Yan, D.F. Xue, J. Phys. Chem. B 110 (2006) 7102.
[19] X.B. Cao, X.M. Lan, Y. Guo, C. Zhao, S.M. Han, J. Wang, Q.R. Zhao, J. Phys. Chem. C 111 (2007) 18958.
[20] Y.H. Ni, S. Yang, J.M. Hong, L. Zhang, W.L. Wu, Z.S. Yang, J. Phys. Chem. C 112 (2008) 8200.
[21] Z. Chen, Q.M. Gao, M.L. Ruan, Nanotechnology 18 (2007) 255607.
[22] R. Yi, R.R. Shi, G.H. Gao, N. Zhang, X.M. Cui, Y.H. He, X.H. Liu, J. Phys. Chem. C 113 (2009) 1222.
[23] Y. Chang, J.J. Teo, H.C. Zeng, Langmuir 21 (2005) 1074.
[24] H.J. Fan, U. Gösele, M. Zacharias, Small 3 (2007) 1660.
[25] L. Au, X.M. Lu, Y.N. Xia, Adv. Mater. 20 (2008) 2517.
[26] J. Liang, J. Liu, Q. Xie, S. Bai, W. Yu, Y. Qian, J. Phys. Chem. B 109 (2005) 9463.
[27] J.X. Duan, X.T. Huang, E. Wang, H.H. Ai, Nanotechnology 17 (2006) 1786.
[28] L. Dai, X.L. Chen, W.J. Wang, T. Zhou, B.Q. Hu, J. Phys. Condens. Matter 15 (2003) 2221.
[29] F. Li, Y. Jiang, L. Hu, L.Y. Liu, Z. Li, X.T. Huang, J. Alloys Compd. 474 (2008) 531.
[30] L. Yu, X.F. Yu, Y.F. Qiu, Y.J. Chen, S.H. Yang, Chem. Phys. Lett. 465 (2008) 272.
[31] P. Reiss, M. Protière, L. Li, Small 5 (2009) 154.
[32] A. Datta, S.K. Panda, S. Chaudhuri, J. Phys. Chem. C 111 (2007) 17260.
[33] R.G. Xie, U. Kolb, J.X. Li, T. Basche, A. Mews, J. Am. Chem. Soc. 127 (2005) 7480.
[34] C.L. Jiang, W.Q. Zhang, G.F. Zou, W.C. Yu, Y.T. Qian, Mater. Chem. Phys. 103 (2007) 24.